Classification of Rhythmic Cortical Activity Elicited by Whole-Body Balance Perturbations Suggests the Cortical Representation of Direction-Specific Changes in Postural Stability

Teodoro Solis-Escalante, *Member, IEEE*, Digna de Kam, and Vivian Weerdesteyn

***Abstract*— Postural responses that effectively recover balance following unexpected postural changes need to be tailored to the characteristics of the postural change. We hypothesized that cortical dynamics involved in top-down regulation of postural responses carry information about directional postural changes (i.e., sway) imposed by sudden perturbations to standing balance (i.e., support surface translations). To test our hypothesis, we evaluated the single-trial classification of perturbation-induced directional changes in postural stability from high-density EEG. We analyzed EEG recordings from six young able-bodied individuals and three older individuals with chronic hemiparetic stroke, which were acquired while individuals reacted to low-intensity balance perturbations. Using common spatial patterns for feature extraction and linear discriminant analysis or support vector machines for classification, we achieved classification accuracies above random level ($p < 0.05$; cross-validated) for the classification of four different sway directions (one vs. the rest scheme). Screening of spectral features (3-50 Hz) revealed that the highest classification performance occurred when low-frequency (3-10 Hz) spectral features were used. Strikingly, the participant-specific classification results were qualitatively similar between young able-bodied individuals and older individuals with chronic hemiparetic stroke. Our findings demonstrate that low-frequency spectral components, corresponding to the cortical theta rhythm, carry direction-specific information about changes in postural stability. Our work presents a new perspective on the cortical representation of postural stability and the possible role of the theta rhythm in the modulation of (directional) reactive balance responses. Importantly, our work provides preliminary evidence that the cortical encoding of direction-specific changes in postural stability is present in chronic hemiparetic stroke.**

***Index Terms*— Balance control, common spatial patterns, electroencephalogram (EEG), mobile brain/body imaging (MoBI), Theta rhythm.**

Manuscript received May 7, 2020; revised September 9, 2020; accepted September 28, 2020. Date of publication October 6, 2020; date of current version November 6, 2020. This work was supported by the Netherlands Organization for Scientific Research (NWO) through the project "Roads to Recovery" under VIDI Grant (91717369) PI: Vivian Weerdesteyn. *(Corresponding author: Teodoro Solis-Escalante.)*

Teodoro Solis-Escalante and Digna de Kam are with the Department of Rehabilitation, Donders Institute for Brain, Cognition, and Behavior, Radboud University Medical Center, 6500HB Nijmegen, The Netherlands (e-mail: teodoro.solisescalante@radboudumc.nl).

Vivian Weerdesteyn is with the Department of Rehabilitation, Donders Institute for Brain, Cognition, and Behavior, Radboud University Medical Center, 6500HB Nijmegen, The Netherlands, and also with Sint Maartenskliniek Research, 6500GM Nijmegen, The Netherlands.

Digital Object Identifier 10.1109/TNSRE.2020.3028966

I. Introduction

HUMAN standing balance and upright posture are maintained through interactions of hierarchically organized and highly interconnected neural ensembles distributed across the central nervous system (CNS), including the cerebral cortex [1], [2]. Initial automatic postural responses are presumably mediated by brainstem/midbrain structures, and the possible cortical contributions to reactive postural responses likely increase with the latency of such responses [3]. The cortical responses to balance perturbations appear in the electroencephalogram (EEG) between 30 and 400 ms after perturbation onset, with a broad scalp distribution and a rich spectral composition [4]–[6]. The cortical responses may reflect concurrent cognitive and sensorimotor processes related to the integration of the multisensory input (visual, vestibular, and proprioceptive) associated with sudden postural changes [7], [8] and to the detection of a mismatch between expected and current postural stability, as a form of error detection [9], [10] or sensorimotor conflict [4]. In turn, the later cortical responses could represent direct contributions to the reactive postural responses [2], [3].

Recent studies on mobile brain/body imaging (MoBI) based on high-density EEG identified consistent patterns of rhythmic neural activity that could support the detection of a mismatch between expected and current postural stability [4], [5], [11]. First, soon after perturbation onset, a transient enhancement of the theta (3-7 Hz) rhythm appears in frontal, central, parietal, and occipital cortical areas, irrespective of the sensory modality of the perturbation (visual or physical perturbations; [4]) or the subsequent postural response (stepping or maintaining both feet in place; [5]). A similar pattern has been observed during a balance beam walking task during the double support phase of the gait cycle directly preceding the loss of

balance [11], when proprioceptive information from both feet could be used for assessment of postural stability. The broad spatial distribution of the theta enhancement suggests cortico-cortical interactions that may support the integration of sensory information. Second, a transient enhancement of theta, alpha (8-12 Hz), and beta (13-17 Hz) rhythms appears in midline central cortical areas following physical perturbations [4], [5] and in parietal cortical areas following visual perturbations, i.e., brisk rotation of the visual field in a virtual environment [4]. This pattern was first identified in frontal and central scalp areas as the spectral components of the main cortical evoked response to physical balance perturbations [12], and also around the onset of voluntary balance reactions during unperturbed postural sway [13]. Interestingly, the presence of similar broadband patterns in central and parietal areas suggest consistent neural mechanisms for balance control that are common across sensory modalities of the perturbation. These common cortical mechanisms could represent the integration of multisensory information related to postural stability for adaptation of late-phase responses (e.g. stepping or reaching for support [2], [3]).

Because reactive postural responses are known to be direction-specific [14]–[16], we hypothesized that cortical processes involved in (feedback) control of balance and posture convey direction-specific information further into the CNS, presumably for appropriate modulation and execution of reactive postural responses. Our goal was to determine if the modulations of rhythmic neural activity elicited by whole-body balance perturbations carry information related to direction-specific changes in postural stability. To achieve this goal, we evaluated the offline single-trial classification of four different sway directions based on high-density EEG. We analyzed a database of EEG recordings from six young able-bodied individuals and three older individuals with chronic hemiparetic stroke. Importantly, the focus of our analysis was the single-trial classification of sway direction within each participant.

Individuals with chronic hemiparetic stroke were included because their reduced balance capacity towards one body side, demonstrated by greater postural sway towards the paretic side in response to balance perturbations of equal intensity, and associated to direction-specific deficits in their neuromuscular responses [14]. In individuals with chronic hemiparetic stroke, cortical activity related to balance control could reflect both primary cortical deficits and/or the long-term adaptation of the cortical representation of postural stability due to the acquired asymmetric balance capacity. We expected that the inclusion of individuals with chronic hemiparetic stroke would indicate if cortical encoding of direction-specific changes in postural stability exists after stroke. Such knowledge is necessary to guide further studies on cortical correlates of impaired balance capacity post-stroke, and for the development of future EEG-based systems for monitoring of postural stability.

II. Materials and Methods

A. Database Description

We analyzed a database of high-density EEG recordings from six young able-bodied individuals and three older individuals with chronic hemiparetic stroke who participated in one experimental session with a reactive balance task. The experiments were undertaken with the understanding and written consent of each individual. The study protocol was approved by the ethics committee of the Medisch Spectrum Twente (Enschede, The Netherlands; NL52632.044.15). The experiments were conducted in accordance with the Declaration of Helsinki.

B. Participants

Six young able-bodied volunteers (age 26.3 $\pm$ 1.6 years, 2 female) were recruited for the experiment. None of them had self-reported history of neurological or neuromuscular disease, or any other impairments that limited their involvement in the experiment. In addition, three older individuals with chronic hemiparetic stroke (male) were recruited. The individuals with stroke had mild to moderate motor impairments caused by unilateral supratentorial lesions and were able to stand and walk independently on uneven terrain (functional ambulation category score of 5). None of the individuals with stroke presented other neurological, cognitive, or musculoskeletal impairments. Table I and Table II show the participants' characteristics.

C. Experimental Paradigm

The experiments were conducted with the Radboud Falls Simulator, a dynamic posturography system for delivering multidirectional balance perturbations [17]. During the experiments, participants stood in the middle of a movable platform with a narrow stance (feet approximately 4.5 cm apart). The participants were instructed to maintain standing balance in response to low-intensity balance perturbations, i.e. translations of the movable platform in the horizontal plane. The perturbation consisted of constant acceleration (300 ms), constant velocity (500 ms), and constant deceleration (300 ms). The acceleration was 0.5 m/s^2. At this acceleration, the low-intensity of the perturbations required feet-in-place responses for maintaining standing balance. After the perturbation, the platform remained stationary for two seconds before slowly returning to its initial position. For safety reasons, individuals with chronic hemiparetic stroke were fitted with a safety harness (ARG 110 ERGOTEC, SKYLOTEC GmbH, Neuwied, Germany) and an ankle brace (ASO, Medical Specialties, Wadesboro, NC, USA) on the paretic side, which only provided minimal support.

During the experiment, the participants were perturbed with movements of the support surface in four different directions (see Fig. 1). The support surface translations cause the body to sway in the opposite direction of the surface movement. In this study, we refer to sway direction (i.e., the direction of loss of balance) rather than perturbation direction to emphasize that the cortical responses indicate changes in body posture. The directions were identified in a previous study [14] as the directions with preferential recruitment of coordinated muscular responses during reactive balance control. The experiment included 50 trials per direction, for a total of 250 trials divided into five blocks with ten trials per direction. The order of the directions was randomized. The onset of the perturbation within each block varied between 10 and 12 s. Task

TABLE I
CHARACTERISTICS OF ABLE-BODIED INDIVIDUALS

	Gender	Preferred stepping leg	Age (years)	Number of trials			
				FWD P	FWD N	BWD P	BWD N
P1	M	R	25	50	48	50	46
P2	F	L	27	47	45	48	44
P3	F	R	25	46	48	47	45
P4	M	L	29	47	48	49	48
P5	M	R	27	46	49	50	45
P6	M	R	25	48	46	49	42

FWD P: forward preferred leg; FWD N: forward non-preferred leg
BWD P: backward preferred leg; BWD N: backward non-preferred leg

TABLE II
CHARACTERISTICS OF INDIVIDUALS WITH CHRONIC HEMIPARETIC STROKE

	Paretic side *	Age (years)	Years after stroke	FMA	BBS	Number of trials			
						FWD P	FWD N	BWD P	BWD N
P7	R	52	6	28	56	46	47	39	40
P8	L	74	11	24	56	44	40	42	41
P9	L	52	8	30	56	50	38	49	48

* Paretic side is contralateral to the lesioned brain hemisphere
FMA: Fugl-Meyer Assessment of motor recovery after stroke (0-34 points)
BBS: Berg balance scale (0-56 points)
FWD P: forward paretic leg; FWD N: forward non-paretic leg
BWD P: backward paretic leg; BWD N: backward non-paretic leg

performance was visually evaluated and manually annotated during data acquisition.

D. Data Acquisition

High-density EEG was recorded using a cap with 126 Ag-AgCl electrodes (WaveGuard, ANT Neuro, Hengelo, The Netherlands), distributed across the scalp according to the five percent electrode system [18]. The EEG was referenced to the common average during acquisition. The ground electrode was placed on the left mastoid. A biosignal amplifier (REFA System, TMSi, Oldenzaal, The Netherlands) recorded the EEG at 2048 Hz without any filters, except for a built-in antialiasing low-pass filter. To monitor for physiological artifacts, two-channel electrooculogram (EOG) was recorded with the same amplifier using adhesive Ag-AgCl electrodes placed slightly above the nasion (vertical eye movement) and at the outer canthus of the left eye (horizontal eye movement). The onset of each perturbation trial was recorded from a synchronization trigger generated by the platform controller.

E. EEG Analysis

1) Preprocessing: The EEG was analyzed with MATLAB (The Mathworks, Inc., Natick, MA, USA) using custom scripts and incorporating functions from EEGLAB [19]. The EEG was bandpass filtered between 2 and 200 Hz (4^{th} order Butterworth IIR filter, zero-phase shift) and downsampled to 512 Hz. Highly contaminated channels were identified by visual inspection and removed from the recordings. On average, 126 channels remained for analysis (SD $\pm$ 1.6; range: 123-128). The remaining channels were re-referenced to the common average.

2) Artifact Correction: To improve the signal-to-noise ratio of the cortical activity contained in the EEG, artifact correction was performed in four stages (see Fig. 2). In the first stage, line noise (50 Hz) and its harmonics (100 Hz and 150 Hz) were removed with the *CleanLine* plugin for EEGLAB, which uses frequency-domain regression to estimate and reduce sinusoidal artifacts.

In the second stage, nonstationary high-amplitude artifacts (e.g., muscle artifacts, eye movements, and electrode movements) were reduced with the *clean_rawdata* plugin for EEGLAB, which implements the artifact subspace reconstruction (ASR) method [20]. This method determines statistical parameters from a signal subspace obtained from principal component analysis (PCA) of *artifact-free* EEG. To identify artifacts, new statistical parameters are determined from sliding-window PCA and compared against the parameters from the signal subspace. When artifacts are identified, the corresponding principal components (i.e., the artifact subspace) are suppressed, and artifact-reduced EEG is reconstructed for the corresponding sliding window. In this stage, the signal subspace was automatically determined by the *clean_rawdata* plugin from the continuous participant-specific dataset, including all intertrial intervals where participants stood quietly and the support surface remained stationary. We used a rejection threshold of 10 $\times$ SD of the signal subspace parameters and allowed for rejection of segments if more than 50% of the channels are judge outside the signal subspace.

In the third stage, the EEG was segmented into epochs from -2 to 3 s relative to perturbation onset. Based on manual annotations during data acquisition, epochs corresponding to incorrect task execution were discarded. Infomax independent component analysis (ICA), implemented in EEGLAB, decomposed the epoched EEG into maximally independent and spatially stationary components, corresponding to cortical source-level activity and remaining artifacts. Because re-referencing the EEG to the common average reduces the rank of the data by one, PCA was applied to the epoched EEG and the component with zero-valued eigenvalue was removed before computing ICA.

ICA was used for artifact correction. Therefore, we identified the independent components (ICs) most likely to represent artifact-related activity and remove those ICs from the data. Artifact-related ICs were identified by the median frequency of their power spectrum ($\geq$25 Hz), their correlation coefficient with the EOG channels ($\geq$0.6), and the topography of their scalp projection (major contributions of one single electrode). The artifact-related components were removed and artifact-reduced EEG was reconstructed. On average, the artifact-reduced EEG consisted of 47 independent components (SD $\pm$ 11.4; range: 30-69).

In the fourth stage, the impact of task-related muscle activity was further reduced by computing a set of spatial filters that enhance the contributions of low frequency cortical rhythms and minimize the contributions of broadband high frequency

rhythms (assumed to represent muscle artifacts). The spatial filters were obtained from the generalized eigendecomposition between the covariance matrices of lowpass (zero-phase shift FIR order 103, 25 Hz) and bandpass (zero-phase shift FIR order 103, 25 to 100 Hz) filtered EEG [21]. The generalized eigendecomposition

$$\boldsymbol{W} \cdot \boldsymbol{\Lambda} = \boldsymbol{\Sigma}_R^{-1} \cdot \boldsymbol{\Sigma}_A \cdot \boldsymbol{W} \tag{1}$$

finds the eigenvectors $\boldsymbol{W}$ that maximize the ratio (eigenvalues $\boldsymbol{\Lambda}$) between $\boldsymbol{\Sigma}_A$ and $\boldsymbol{\Sigma}_R$, which in this case correspond to the covariance matrices of lowpass and bandpass filtered EEG. The covariance matrices were computed from the filtered EEG after extracting and concatenating a one-second time window directly after perturbation onset in each trial (all conditions). Because the rank of the data was reduced after removing independent components in stage three of the artifact correction, the covariance matrices were regularized to the identity matrix according to $\boldsymbol{\Sigma} = (1-\gamma) \cdot \boldsymbol{\Sigma} + \gamma \cdot \boldsymbol{I}$; where $\boldsymbol{\Sigma}$ represents the covariance matrix, $\boldsymbol{I}$ represents the identity matrix, and γ is the regularization parameter ($\gamma = 0.001$). To minimize broadband high frequency rhythms the eigenvectors associated with the five smallest eigenvalues were removed, and the remaining eigenvectors (i.e., spatial filters) were kept for further use in the analysis.

F. Classification of Directional Changes in Postural Stability

The classification followed a *one vs. the rest* scheme, where four different binary classifiers were trained to classify trials from one of the sway directions against trials from the other three (i.e., the rest). This scheme helped to determine if the different balance perturbations elicited cortical responses encoding direction-specific changes in postural stability.

To evaluate classification performance, we computed the classification accuracy (ACC) and the area under the receiver operating characteristic curve (AUC) with 10 × 10-fold cross-validation. This means that the participant-specific data from each sway direction was divided into ten subsets. In each cross-validation fold, nine subsets from each class (i.e., sway direction) were used for feature extraction and classifier training and the remaining subset from each class was used for classifier testing. The ACC and AUC were computed after all ten subsets had been tested (i.e., in the outer folds). In the next (outer) cross-validation fold, the order of the trials was shuffled, respecting class membership, and the (inner) cross-validation was repeated.

1) Feature Extraction: Discriminative features were extracted from the EEG using a variant of the common spatial patterns algorithm (CSP) [22], [23]. For binary classification, the CSP algorithm computes optimal spatial filters that maximize the variance of one of the classes while minimizing the variance of the other classes. This is equivalent to solving (1) for the intra-class covariance matrices. In this implementation, the EEG was passed through the spatial filters of the artifact correction phase and bandpass filtered. Then, covariance matrices were computed from the trials in the training set of each sway direction and regularized

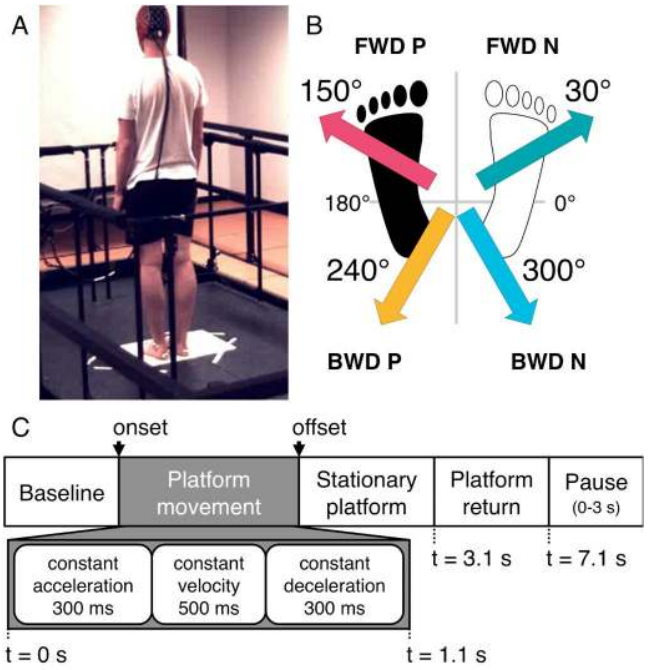

Fig. 1. Experimental setup and paradigm timing. A. Participants stood on a movable platform with a narrow stance. Their task was to maintain standing balance with both feet in place. B. Low-intensity balance perturbations induced postural sway in four different directions (arrows). The sway direction labels indicate forward (FWD), backward (BWD), preferred/paretic body side (P; black foot), or non-preferred/non-paretic body side (N; white foot). C: The balance perturbations were support surface translations with three phases: constant acceleration, constant velocity, and constant deceleration.

($\gamma = 0.001$). The *one vs. the rest* CSP filters were obtained by computing a generalized eigendecomposition using the covariance matrix of one direction and the sum of the covariance matrices of the other directions.

We extracted spectral features between 3 and 50 Hz (in 30 steps, logarithmically spaced). We used the convolution of each EEG epoch with a set of complex Morlet wavelets, which were defined as complex sine waves tapered by a Gaussian [24]. The full-width at half-maximum (FWHM) for these wavelets ranged from 500 to 200 ms, decreasing with increasing wavelet peak frequency. In this way, the wavelets corresponded to a spectral FWHM range of 1.9 to 5.1 Hz. To compute the (regularized) covariance matrices, short time-segments were matched to the FWHM of each wavelet, with an offset of 50 ms relative to perturbation onset.

The resulting CSP filters were combined with the GED spatial filters from the artifact correction phase by multiplying both filter matrices. Actual features for classification were obtained from the first three and the last three spatial filters in the combined filter matrix. Specifically, the artifact-corrected EEG passed through the six spatial filters and the corresponding complex wavelet. Then, the absolute squared was computed for each (complex) time sample, which was log-transformed and smoothed by a 100 ms moving average filter (zero-phase shift). These logarithmic bandpower feature vectors had six features.

2) Classification: Binary classification was handled by linear discriminant analysis (LDA) and support vector machines (SVM). These classifiers are the most popular for single-trial

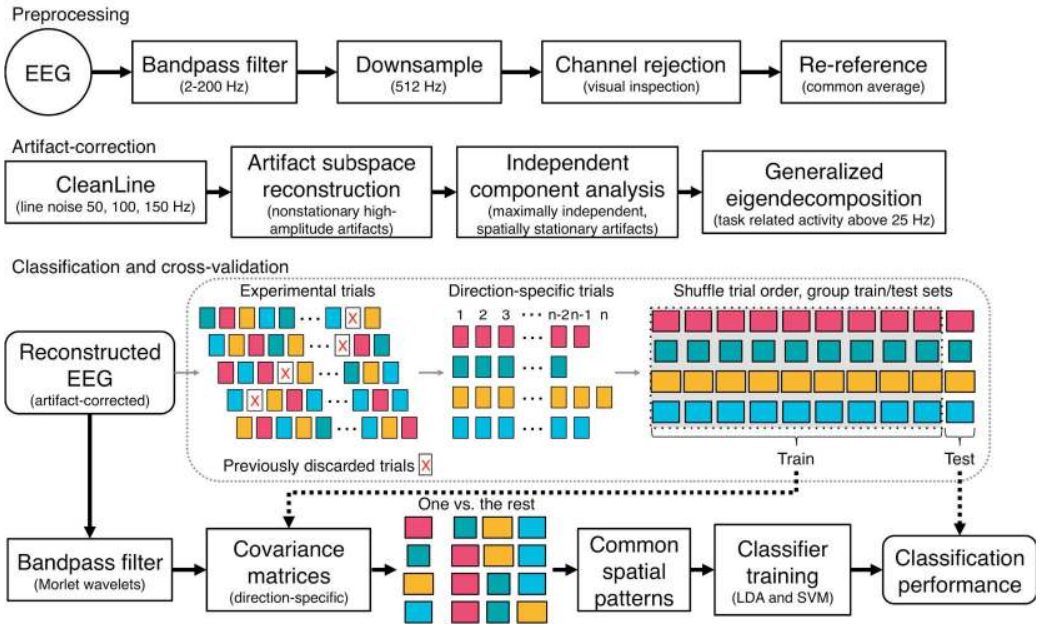

Fig. 2. Diagram of EEG preprocessing, artifact correction, and classification.

classification in the field of brain-computer interfaces [25]. The LDA is a linear classifier that provides a Bayes-optimal separating hyperplane based on the class means and inter-, intra-class covariance matrices [26]. The SVM is a linear classifier that finds an optimal separating hyperplane by maximizing the margin between this hyperplane and the feature vectors that define the border between both classes (i.e., the support vectors) [26]. The SVM can provide linear separation hyperplanes following a non-linear transformation of the feature space via a kernel function. This can improve the performance in non-linearly separable classification problems.

We used LDA and SVM with linear and Gaussian (radial basis function, rbf) kernels. Noteworthy, the class covariance matrices necessary for LDA were regularized ($\gamma = 0.05$). Regularization of the covariance matrices is more effective for classification and more robust for small training sets [25], [26].

For classifier training, feature vectors were computed as the mean value of the continuous features over the frequency-specific time-segments used for feature extraction (matched to the FWHM). For classifier testing, the classifiers were applied to the sample-by-sample features in each testing trial. Class membership was determined by majority vote on the sign of the sample-by-sample classification within the frequency-specific time-segments.

3) Statistical Analyses: The statistical significance of participant-level classification accuracy was determined with non-parametric permutation statistics [27], [28]. The classification accuracy of each cross-validation test (i.e., the outer folds) was compared against a surrogate distribution of random accuracies created via random permutations (n = 200) of the *true* class labels. The random accuracy level was defined from the 95th percentile of the surrogate distribution of random accuracies. At participant-level, statistically significant differences between classification accuracy (cross-validated) and the random accuracy level were calculated using non-parametric one-tailed Wilcoxon signed rank tests ($\alpha = 0.05$).

Also at participant-level, the performance of the different classifiers (LDA, SVM-lin, SVM-rbf) was evaluated with a non-parametric one-way Kruskal-Wallis. Multiple comparisons between classifier-specific performance were conducted using non-parametric two-tailed Wilcoxon signed rank tests. The significance level ($\alpha = 0.05$) for multiple comparisons was corrected for false discovery rate (FDR) [29]. These analyses were repeated for each spectral feature and sway direction.

G. Spatial Patterns

All classifiers were trained with features extracted using participant-specific and direction-specific spatial filters. Each of these filters can be associated with a spatial pattern that represents the scalp projection of the underlying cortical sources [30]; therefore allowing for interpretation regarding the neurophysiological origin of the discriminative features. For each participant, the spatial patterns from all cross-validation folds were averaged (respecting the filter order) after taking the absolute value and normalizing each pattern by its root mean square. For group-level visualization, the spatial patterns of young able-bodied individuals were clustered with the k-means algorithm (k = 3; metric: cosine distance). This was separately done for the first three (i.e., direction-specific) and the last three spatial filters (i.e., *rest* class). The spatial patterns of the individuals with chronic hemiparetic stroke were excluded from group-level pattern visualization.

III. Results

A. Classification Accuracy

Table I and Table II show the participant-specific number of trials per direction available for classification. Fig. 3 presents the mean classification accuracy (over cross-validation folds)

achieved for each participant, sway direction, spectral feature, and classifier type. Overall, the classification accuracy was consistently above the random level for features extracted from low-frequency spectral components, in both healthy young able-bodied individuals and older individuals with chronic hemiparetic stroke. On the other hand, high-frequency spectral components yielded classification accuracies above the random level for some, but not all, participants. Comparisons between classifiers (Fig. 3) showed that the highest accuracies were obtained by the SVM classifiers, but the differences between linear and Gaussian kernels were not always significant.

Noteworthy, the mean random accuracies across participants and spectral features were LDA 55.3% (SD 1.0%), SVM-lin 72.0% (SD 2.0%), and SVM-rbf 73.5% (SD 1.9%). The higher random accuracy levels of the SVM classifiers show that the outputs of these are less affected by random permutations of the true class labels, which suggests a bias towards the more prevalent class. This effect is better appreciated from the confusion matrices.

Fig. 4 presents a set of mean confusion matrices, averaged across young able-bodied individuals, and corresponding to spectral features with non-overlapping frequency bands. The confusion matrices show that the SVM classifiers lead to a high proportion of true and false negatives. This is evident for high-frequency spectral components, which resulted in classification accuracies not significantly above random accuracy levels. Nonetheless, the results presented in Fig. 3 and Fig. 4 demonstrate that classification accuracies above chance level are achieved when features are extracted from low-frequency spectral components. Furthermore, the estimation of random accuracy level is able to handle the class imbalance of the *one vs the rest* scheme.

B. Area Under the Receiver Operating Characteristic Curve

Fig. 5 presents the mean area under the receiver operating characteristic curve (over cross-validation folds) estimated for each participant, spectral feature, and classifier type. The AUC gives complementary information about a classifier's ability to separate the positive and negative classes and it is robust against class imbalance, i.e., a random level of performance results in 0.5 AUC, regardless of class prevalence.

The results in Fig. 5 show that, overall, the AUC was higher for features extracted from low-frequency spectral components, in both young able-bodied individuals and older individuals with chronic hemiparetic stroke; in a similar way that the results for classification accuracy. Comparisons between classifiers in terms of AUC showed that highest performances were obtained by the linear classifiers, i.e., LDA and SVM with a linear kernel. Moreover, an effect of classifier type was uncommon (c.f. classification accuracy in Fig. 3). These results show that the classification problem can be solved using linear classifiers.

C. Scalp Topography of the Spatial Patterns

Fig. 6 presents the spatial patterns associated with direction- and frequency-specific spatial filters for extraction of spectral features. The spatial patterns are shown for the evaluation of LDA classifiers and the set of features presented in Fig. 4. The spatial patterns were obtained as group-level visualization via k-means clustering of the spatial patterns of young able-bodied individuals. Notably, the spatial patterns of low-frequency spectral components present scalp topographies with clear fronto-centro-parietal distributions.

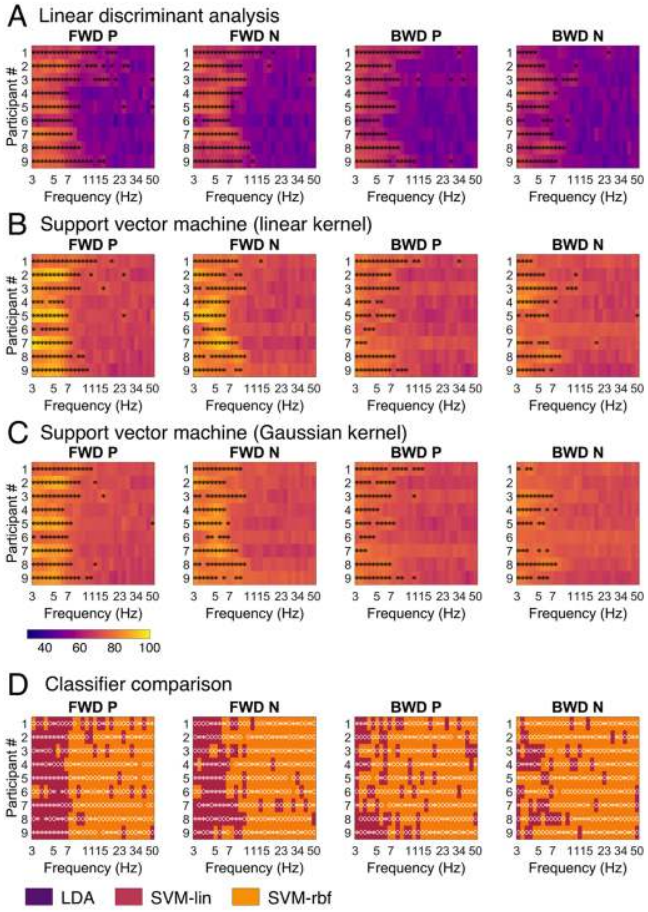

Fig. 3. Classification accuracy. A–C. Cross-validated mean classification accuracy per participant, sway direction, spectral feature, and classifier type. Images shown with the same color scale. Accuracies above random level ($p < 0.05$, FDR corrected) are indicated with black asterisks. D. Tile colors corresponding to the classifier type with highest accuracy. Results of multiple comparisons ($p < 0.05$, FDR corrected) indicate accuracy significantly higher than the other two classifiers (white asterisks), accuracy significantly higher than one other classifier (white diamonds), non-significant differences (white plus signs). Tiles without markers indicate no effect of classifier type. Participant 1-6: young able-bodied individuals. Participant 7-9: older individuals with chronic hemiparetic stroke.

IV. Discussion

A. Low-Frequency Spectral Components Encode Direction-Specific Changes to Postural Stability

The key finding in our study is that direction-specific changes in postural stability can be classified from modulations of low-frequency spectral components (3-10 Hz) of the EEG (see Fig. 3 and Fig. 5). Remarkably, these modulations were identified in young able-bodied individuals and three older individuals with unilateral cerebral lesions (chronic

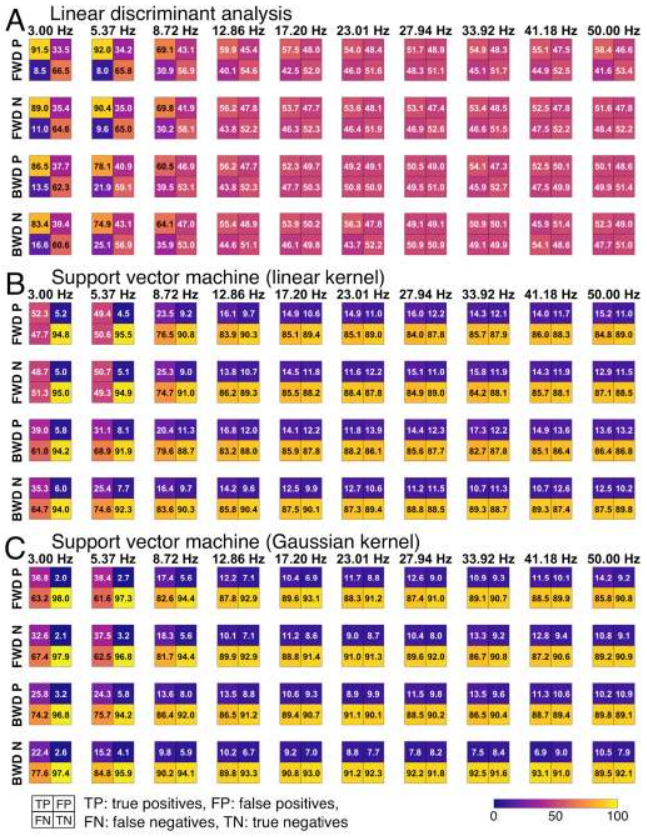

Fig. 4. Confusion matrices. To summarize the performance of the LDA and SVM classifiers the participant-specific confusion matrices were averaged across young able-bodied individuals (Participant 1-6). These matrices suggest a bias towards the negative class (*the rest*) in the SVM classifiers.

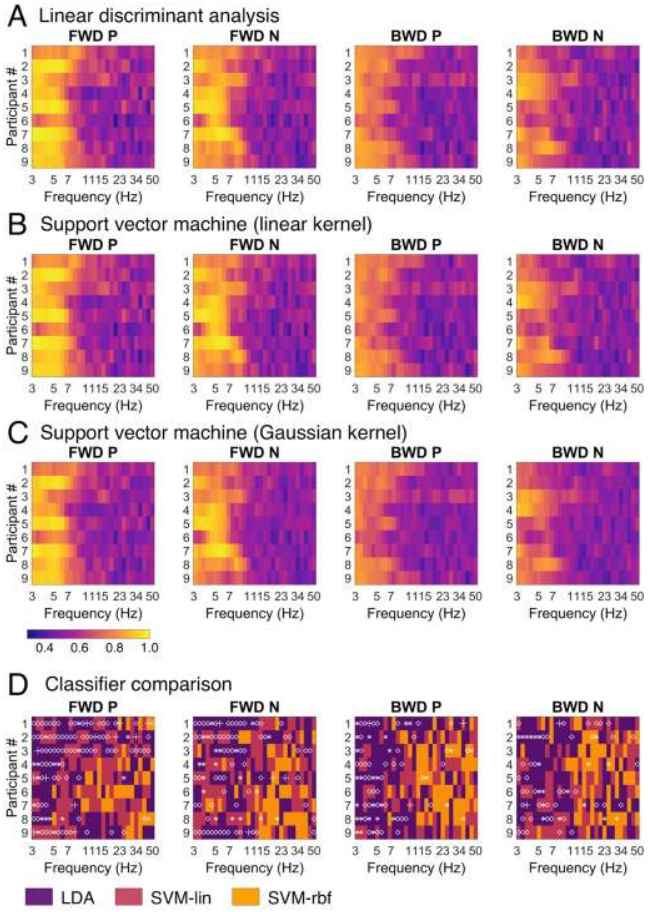

Fig. 5. Area under the receiver operating characteristic curve. A–C. Cross-validated mean AUC per participant, sway direction, spectral feature, and classifier type. Images shown with the same color scale. D. Tile colors corresponding to the classifier type with highest AUC. Results of multiple comparisons ($p < 0.05$, FDR corrected) indicate AUC significantly higher than the other two classifiers (white asterisks), AUC significantly higher than one other classifier (white diamonds), non-significant differences (white plus signs). Tiles without markers indicate no effect of classifier type. Participant 1-6: young able-bodied individuals. Participant 7-9: older individuals with chronic hemiparetic stroke.

hemiparetic stroke). Our finding demonstrates an association between the low-frequency (e.g., theta rhythm) cortical rhythms and the cortical representation of postural stability; presumably for the appropriate selection and/or modulation of direction-specific postural responses.

The low-frequency rhythms may represent the detection of a mismatch between expected and (imposed changes to) current postural stability, which has been previously considered a form of error detection or processing of sensorimotor conflict [4], [6], [9], [10]. This interpretation is consistent with a view of the theta rhythm as representing mechanisms of cognitive control for the self-regulation of behavior [31]–[36]. Indeed, many studies have found correlations between modulations of the (fronto-central) theta rhythm and task performance in experiments related to action monitoring (i.e., the capacity to evaluate the outcome of one's actions in order to detect errors and initiate corrective adjustments) and the resolution of response conflict (i.e., the ability to select task-relevant responses among competing alternatives) [31]–[39]. Although our experimental paradigm did not required overt motor responses, the postural control system (likely involving the cerebral cortex) could have assessed the direction of postural sway, in order to determine an appropriate postural response for maintaining balance. Interestingly, recent studies on cortical control of balance and posture have found that the power of the fronto-central theta rhythm covaries with the postural demand of a continuous "feet-in-place" balance task [40]–[42]. Based on these observations and the presently found relevance of the theta rhythm for the classification of direction-specific sway, we suggest that the cortical theta rhythm may play a role in the feedback control of balance and posture.

B. The Cortical Representation of Postural Stability Includes the Medial Frontal Cortex

Another relevant finding in our study is that the cortical representation of direction-specific changes in postural stability (related to low-frequency spectral components) appeared with well-defined scalp topographies showing fronto-centro-parietal distributions (Fig. 6), which is consistent with previous studies on cortical control of balance [4]–[6], [41], [42]. Furthermore, the fronto-central topography of the theta rhythm is a hallmark of cognitive control [35], [36], [38].

Notably, spatial patterns clustered across young able-bodied individuals show subtle differences in the scalp topography of the multiple sway directions (c.f. positive and negative classes in Fig. 6). This could indicate that the direction

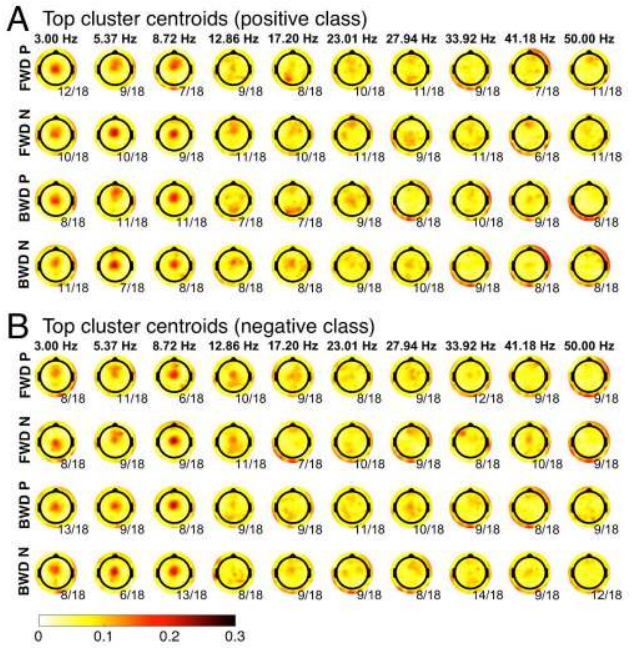

Fig. 6. Spatial patterns of young able-bodied individuals (Participant 1-6). These spatial patterns represent centroids of the most common clusters of direction- and frequency-specific spatial filters used for feature extraction of the positive (A) and negative (B) classes. Noteworthy, the low-frequency spectral components, related to the best classification performance, show well-defined topographies.

of a change in postural stability is encoded by precisely timed differential power modulations of the theta rhythm across adjacent structures in the medial prefrontal cortex, e.g., the anterior cingulate cortex and the supplementary motor area [35], [43], [44]; without dismissing possible contributions from other cortical areas [4], [5]. Furthermore, coordination between multiple (near and/or distant) cortical areas may be required for effective postural control. Thus, the direction of a change in postural stability may also be encoded in patterns of neural synchronization across the cerebral cortex. Such neural synchronization patterns could not be revealed in our study because the analyses were based on power modulations. Nonetheless, recent studies have shown reorganization of cortico-cortical synchronization in the frequencies of the theta rhythm following perturbations to standing balance [41], [45], [46]. Notably, Peterson and Ferris [46] found that the supplementary motor area could serve as a hub for a cortical sensorimotor network relevant for the control of balance and posture. This is consistent with a role of the fronto-central theta rhythm as part of a feedback control system for balance and posture.

C. Decoding Direction-Specific Changes to Postural Stability in Individuals With Chronic Stroke – Preliminary Evidence

Our study shows that the classification of direction-specific changes to postural stability using spectral components of the EEG is feasible. This was demonstrated in a small group of young able-bodied individuals and, remarkably, also in three older individuals with chronic hemiparetic stroke.

The analysis of experimental data from individuals with chronic hemiparetic stroke provides preliminary evidence on persisting cortical encoding of direction-specific changes in postural stability after stroke. These preliminary findings encourage pursuing future systematic investigation of cortical sensitivity to sway direction and its possible relation with participant-specific balance impairments due to stroke, other neurological conditions (such as Parkinson's disease), or due to age-related decline.

V. Conclusion

Our study demonstrates that modulations of low-frequency spectral components of the EEG encode information about the direction of an imposed change to postural stability. The scalp topographies associated with the spectral features leading to the highest classification performance suggest a role of the fronto-central theta rhythm in the cortical representation of postural stability. Online monitoring of the fronto-central theta rhythm, perhaps in combination with other perturbation-related features (e.g., the N1 potential [6], [10], [47]) may provide the basis for an EEG-based fall detection system for use in rehabilitation. The inclusion of individuals with chronic hemiparetic stroke in this study presents preliminary evidence of an existing cortical representation of postural stability in individuals with impaired (i.e., asymmetric) balance capacity. Our study provides a new perspective on the cortical representation of postural stability and the possible role of the theta rhythm in the modulation of (directional) reactive balance responses.

Acknowledgment

The authors would like to express their gratitude to Joris van der Cruijsen for assistance with data collection during creation of the database. Funding sources were not involved in study design; in the collection, analysis, and interpretation of data; in the writing of this report; nor in the decision to submit the article for publication.

References

[1] D. A. E. Bolton, "The role of the cerebral cortex in postural responses to externally induced perturbations," *Neurosci. Biobehavioral Rev.*, vol. 57, pp. 142–155, Oct. 2015.
[2] K. Takakusaki, "Functional neuroanatomy for posture and gait control," *J. Movement Disorders*, vol. 10, no. 1, pp. 1–17, Jan. 2017.
[3] J. V. Jacobs and F. B. Horak, "Cortical control of postural responses," *J. Neural Transmiss.*, vol. 114, no. 10, pp. 1339–1348, Oct. 2007.
[4] S. M. Peterson and D. P. Ferris, "Differentiation in theta and beta electrocortical activity between visual and physical perturbations to walking and standing balance," *Eneuro*, vol. 5, no. 4, pp. 1–20, Jul. 2018.
[5] T. Solis-Escalante, J. van der Cruijsen, D. de Kam, J. van Kordelaar, V. Weerdesteyn, and A. C. Schouten, "Cortical dynamics during preparation and execution of reactive balance responses with distinct postural demands," *NeuroImage*, vol. 188, pp. 557–571, Mar. 2019.
[6] J. P. Varghese, R. E. McIlroy, and M. Barnett-Cowan, "Perturbation-evoked potentials: Significance and application in balance control research," *Neurosci. Biobehavioral Rev.*, vol. 83, pp. 267–280, Dec. 2017.
[7] V. Dietz, J. Quintern, W. Berger, and E. Schenck, "Cerebral potentials and leg muscle e.M.g. responses associated with stance perturbation," *Exp. Brain Res.*, vol. 57, no. 2, pp. 348–354, Jan. 1985.
[8] V. Dietz, J. Quintern, and W. Berger, "Cerebral evoked potentials associated with the compensatory reactions following stance and gait perturbation," *Neurosci. Lett.*, vol. 50, nos. 1–3, pp. 181–186, Sep. 1984.

[9] A. L. Adkin, S. Quant, B. E. Maki, and W. E. McIlroy, "Cortical responses associated with predictable and unpredictable compensatory balance reactions," *Exp. Brain Res.*, vol. 172, no. 1, p. 85, 2006.

[10] A. M. Payne, L. H. Ting, and G. Hajcak, "Do sensorimotor perturbations to standing balance elicit an error-related negativity?" *Psychophysiology*, vol. 56, no. 7, Jul. 2019, Art. no. e13359.

[11] A. R. Sipp, J. T. Gwin, S. Makeig, and D. P. Ferris, "Loss of balance during balance beam walking elicits a multifocal theta band electrocortical response," *J. Neurophysiology*, vol. 110, no. 9, pp. 2050–2060, Nov. 2013.

[12] J. P. Varghese, A. Marlin, K. B. Beyer, W. R. Staines, G. Mochizuki, and W. E. McIlroy, "Frequency characteristics of cortical activity associated with perturbations to upright stability," *Neurosci. Lett.*, vol. 578, pp. 33–38, Aug. 2014.

[13] J. P. Varghese, K. B. Beyer, L. Williams, V. Miyasike-daSilva, and W. E. McIlroy, "Standing still: Is there a role for the cortex?" *Neurosci. Lett.*, vol. 590, pp. 18–23, Mar. 2015.

[14] D. de Kam, A. C. Geurts, V. Weerdesteyn, and G. Torres-Oviedo, "Direction-specific instability poststroke is associated with deficient motor modules for balance control," *Neurorehabilitation Neural Repair*, vol. 32, nos. 6–7, pp. 655–666, Jun. 2018.

[15] S. A. Chvatal, G. Torres-Oviedo, S. A. Safavynia, and L. H. Ting, "Common muscle synergies for control of center of mass and force in nonstepping and stepping postural behaviors," *J. Neurophysiol.*, vol. 106, no. 2, pp. 999–1015, Aug. 2011.

[16] G. Torres-Oviedo and L. H. Ting, "Muscle synergies characterizing human postural responses," *J. Neurophysiol.*, vol. 98, no. 4, pp. 2144–2156, Oct. 2007.

[17] J. Nonnekes, D. de Kam, A. C. Geurts, V. Weerdesteyn, and B. R. Bloem, "Unraveling the mechanisms underlying postural instability in Parkinson's disease using dynamic posturography," *Expert Rev. Neurotherapeutics*, vol. 13, no. 12, pp. 1303–1308, Dec. 2013.

[18] R. Oostenveld and P. Praamstra, "The five percent electrode system for high-resolution EEG and ERP measurements," *Clin. Neurophysiol.*, vol. 112, no. 4, pp. 713–719, Apr. 2001.

[19] A. Delorme and S. Makeig, "EEGLAB: An open source toolbox for analysis of single-trial EEG dynamics including independent component analysis," *J. Neurosci. Methods*, vol. 134, no. 1, pp. 9–21, Mar. 2004.

[20] T. R. Mullen *et al.*, "Real-time neuroimaging and cognitive monitoring using wearable dry EEG," *IEEE Trans. Biomed. Eng.*, vol. 62, no. 11, pp. 2553–2567, Nov. 2015.

[21] M. X. Cohen, "Comparison of linear spatial filters for identifying oscillatory activity in multichannel data," *J. Neurosci. Methods*, vol. 278, pp. 1–12, Feb. 2017.

[22] B. Blankertz, R. Tomioka, S. Lemm, M. Kawanabe, and K.-R. Müller, "Optimizing spatial filters for robust EEG single-trial analysis," *IEEE Signal Process. Mag.*, vol. 25, no. 1, pp. 41–56, Dec. 2008.

[23] H. Ramoser, J. Müller-Gerking, and G. Pfurtscheller, "Optimal spatial filtering of single trial EEG during imagined hand movement," *IEEE Trans. Rehabil. Eng.*, vol. 8, no. 4, pp. 441–446, Dec. 2000.

[24] M. X. Cohen, "A better way to define and describe Morlet wavelets for time-frequency analysis," *NeuroImage*, vol. 199, pp. 81–86, Oct. 2019.

[25] F. Lotte *et al.*, "A review of classification algorithms for EEG-based brain–computer interfaces: A 10 year update," *J. Neural Eng.*, vol. 15, no. 3, Jun. 2018, Art. no. 031005.

[26] S. Lemm, B. Blankertz, T. Dickhaus, and K.-R. Müller, "Introduction to machine learning for brain imaging," *NeuroImage*, vol. 56, no. 2, pp. 387–399, May 2011.

[27] E. Maris and R. Oostenveld, "Nonparametric statistical testing of EEG- and MEG-data," *J. Neurosci. Methods*, vol. 164, no. 1, pp. 177–190, Aug. 2007.

[28] T. E. Nichols and A. P. Holmes, "Nonparametric permutation tests for functional neuroimaging: A primer with examples," *Hum. Brain Mapping*, vol. 15, no. 1, pp. 1–25, Jan. 2002.

[29] Y. Benjamini and D. Yekutieli, "The control of the false discovery rate in multiple testing under dependency," *Ann. Statist.*, vol. 29, no. 4, pp. 1165–1188, Aug. 2001.

[30] S. Haufe *et al.*, "On the interpretation of weight vectors of linear models in multivariate neuroimaging," *NeuroImage*, vol. 87, pp. 96–110, Feb. 2014.

[31] J. F. Cavanagh, L. Zambrano-Vazquez, and J. J. B. Allen, "Theta lingua franca: A common mid-frontal substrate for action monitoring processes," *Psychophysiology*, vol. 49, no. 2, pp. 220–238, Feb. 2012.

[32] P. Luu, D. M. Tucker, and S. Makeig, "Frontal midline theta and the error-related negativity: Neurophysiological mechanisms of action regulation," *Clin. Neurophysiol.*, vol. 115, no. 8, pp. 1821–1835, Aug. 2004.

[33] L. T. Trujillo and J. J. B. Allen, "Theta EEG dynamics of the error-related negativity," *Clin. Neurophysiol.*, vol. 118, no. 3, pp. 645–668, Mar. 2007.

[34] P. Luu, T. Flaisch, and D. M. Tucker, "Medial frontal cortex in action monitoring," *J. Neurosci.*, vol. 20, no. 1, pp. 464–469, Jan. 2000.

[35] K. R. Ridderinkhof, "The role of the medial frontal cortex in cognitive control," *Science*, vol. 306, no. 5695, pp. 443–447, Oct. 2004.

[36] M. M. Botvinick, T. S. Braver, D. M. Barch, C. S. Carter, and J. D. Cohen, "Conflict monitoring and cognitive control," *Psychol. Rev.*, vol. 108, no. 3, pp. 624–652, 2001.

[37] M. X. Cohen and T. H. Donner, "Midfrontal conflict-related theta-band power reflects neural oscillations that predict behavior," *J. Neurophysiol.*, vol. 110, no. 12, pp. 2752–2763, Dec. 2013.

[38] J. F. Cavanagh and M. J. Frank, "Frontal theta as a mechanism for cognitive control," *Trends Cognit. Sci.*, vol. 18, no. 8, pp. 414–421, Aug. 2014.

[39] M. X. Cohen, "Midfrontal theta tracks action monitoring over multiple interactive time scales," *NeuroImage*, vol. 141, pp. 262–272, Nov. 2016.

[40] T. Hülsdünker, A. Mierau, C. Neeb, H. Kleinöder, and H. K. Strüder, "Cortical processes associated with continuous balance control as revealed by EEG spectral power," *Neurosci. Lett.*, vol. 592, pp. 1–5, Apr. 2015.

[41] A. Mierau, B. Pester, T. Hülsdünker, K. Schiecke, H. K. Strüder, and H. Witte, "Cortical correlates of human balance control," *Brain Topography*, vol. 30, no. 4, pp. 434–446, 2017.

[42] S. Slobounov, C. Cao, N. Jaiswal, and K. M. Newell, "Neural basis of postural instability identified by VTC and EEG," *Exp. Brain Res.*, vol. 199, no. 1, pp. 1–16, Oct. 2009.

[43] F. Bonini, B. Burle, C. Liegeois-Chauvel, J. Regis, P. Chauvel, and F. Vidal, "Action monitoring and medial frontal cortex: Leading role of supplementary motor area," *Science*, vol. 343, no. 6173, pp. 888–891, Feb. 2014.

[44] M. M. Botvinick, J. D. Cohen, and C. S. Carter, "Conflict monitoring and anterior cingulate cortex: An update," *Trends Cognit. Sci.*, vol. 8, no. 12, pp. 539–546, Dec. 2004.

[45] J. P. Varghese, W. R. Staines, and W. E. McIlroy, "Activity in functional cortical networks temporally associated with postural instability," *Neuroscience*, vol. 401, pp. 43–58, Mar. 2019.

[46] S. M. Peterson and D. P. Ferris, "Group-level cortical and muscular connectivity during perturbations to walking and standing balance," *NeuroImage*, vol. 198, pp. 93–103, Sep. 2019.

[47] J. C. Ditz, A. Schwarz, and G. R. Müller-Putz, "Perturbation-evoked potentials can be classified from single-trial EEG," *J. Neural Eng.*, vol. 17, no. 3, Jun. 2020, Art. no. 036008.